Original Article

DOI: 10.5582/ddt.2022.01061

ENST00000438158 aids ultrasound for predicting lymph node metastasis and inhibits migration and invasion of papillary thyroid carcinoma cells

Hui Liu[1,§], Yixin Shi[1,§], Jia Zhan[1], Yingchun Liu[1], Jing Zhou[2,3,4], Biao Su[1], Yue Chen[1], Ling Wang[2,3,4,*], Lin Chen[1,*]

[1] Department of Ultrasound, Huadong Hospital, Fudan University, Shanghai, China;
[2] Laboratory for Reproductive Immunology, Obstetrics and Gynecology Hospital of Fudan University, Shanghai, China;
[3] The Academy of Integrative Medicine of Fudan University, Shanghai, China;
[4] Shanghai Key Laboratory of Female Reproductive Endocrine-related Diseases, Shanghai, China.

SUMMARY Cervical lymph node metastasis (CLNM) of papillary thyroid carcinoma (PTC) is directly associated with clinical management and prognosis. In this study, we aimed to evaluate the value of conventional ultrasound (US) combined with ENST00000438158 in predicting CLNM of PTC. Fourty-nine PTC patients underwent US examination and US-guided fine needle aspiration (FNA). ENST00000438158 expression in FNA cytological specimens and PTC cell lines was detected using real-time reverse transcription polymerase chain reaction (qRT-PCR). The role of ENST00000438158 expression in the proliferation, migration, invasion, apoptosis, and cell cycle of PTC cells was investigated by Cell Counting Kit-8 (CCK8) and clone formation experiments, transwell assay, and flow cytometry, respectively. Calcification, capsule contact, and low ENST00000438158 expression were independently associated with PTC with CLNM (all $p < 0.05$). The combination of multiple US features was more valuable than a single US feature in predicting CLNM in PTC. Adding ENST0000438158 to US greatly improved the value of differentiation of PTC with or without CLNM. In conclusion, ENST00000438158 is a potential molecular marker for predicting CLNM in PTC. ENST00000438158 combined with US features is highly valuable for predicting CLNM in PTC.

Keywords Ultrasound, papillary thyroid carcinoma, ENST00000438158, cervical lymph node metastasis

1. Introduction

Thyroid cancer is the most frequent endocrine gland malignancy, and its incidence has been increasing substantially over the past few decades. It is predicted to become the fourth most malignant tumor by 2030 in the United States (*1,2*). In most thyroid cancers, papillary thyroid carcinoma (PTC) has less distant metastasis and a good prognosis (*3-6*). However, there are still a few PTC that develop rapidly, with high invasion, local recurrence, and early distant metastasis (*7,8*). Clinical studies have shown that the incidence of cervical lymph node metastasis (CLNM) in the central and lateral cervical compartment was 12-81% and 3.1-65.4%, respectively. Follow-up results after surgery showed that recurrence and metastasis rates were more than 30%. Therefore, CLNM in PTC is directly related to its management and prognosis (*9,10*). In recent years, preventive lymph node dissection has not reduced the local recurrence rate of PTC but has increased the size of the surgical wound, probability of parathyroid injury, recurrent laryngeal nerve injury, and other complications. Therefore, many studies have recommended preventive central lymph node dissection only for PTC with CLNM confirmed before surgery (*11*). Thus, there is an urgent need to develop an accurate and efficient method for predicting CLNM of PTC. Ultrasound (US) is convenient, radiation-free, and inexpensive, making it the preferred method for the detection of CLNM in PTC. Metastatic lymph nodes are commonly characterized by a round shape, absence of an echogenic hilum, hyperechogenicity, microcalcifications, cystic changes, and peripheral vascularity (*11*). A previous meta-analysis reported that the sensitivity of US for central CLNN was only 33%, of which approximately 70% refer to lateral CLNM (*12*).

Previous studies indicated that US missed 33-90% of CLNM in PTC patients (*13,14*). Therefore, in order to improve the level of scientific decision-making for PTC surgery, instead of directly detecting cervical lymph nodes, we focused on the US features of PTC to predict CLNM.

In recent years, molecular markers have become a hot topic in cancer research (*15,16*). Among them, long noncoding RNA (lncRNAs) *i.e.*, noncoding RNA of more than 200 nucleotides in length are considered key regulators of the occurrence and inhibition of many cancers (*17-19*). lncRNAs play a role in cell biological processes, such as cell differentiation, migration, and invasion, especially in cancers (*20-22*). For example, upregulation of the expression level of lncRNA NONHSAT129183 promoted proliferation, migration, and invasion in PTC cell lines (*23*). High expression of ENST00000606790.1 was strongly correlated with aggressive clinicopathological characteristics of PTC (*24*). On the other hand, lncRNA expression was negatively associated with poor prognosis of thyroid cancer, such as lncRNA GAS5 and lncRNA MEG3 (*25,26*).

The lncRNA ENST0000438158 is located on the antisense strand of chromosome 1, with a length of 562 bp, and contains three gene exons, playing the role of enhancer to affect gene expression nearby. Studies have reported that the expression of lncRNA ENST0000438158 is significantly higher in colon cancer tissues than in normal tissues, and its dysregulation is involved in the complicated process of colon cancer development (*27*). Xie *et al.* (*28*) indicated that ENST0000438158 was the target of miR-223-5p, and that miR-223-5p/ENST0000438158 was differentially expressed in osteosarcoma lung metastasis by constructing a competitive endogenous RNA network related to lung metastasis. However, the role of ENST0000438158 in PTC remains unclear. Therefore, ENST00000438158 was selected as the research object in this study to investigate its use as an auxiliary molecular marker to predict CLNM in PTC together with US.

2. Materials and Methods

2.1. Patients

The Ethics Committee of Huadong Hospital authorized this study. The ethical considerations for the study followed the principles of the Declaration of Helsinki. A total of 49 thyroid nodules from 49 consecutive patients (35 women and 14 men) were included in this study from June 2018 to December 2019. All patients were well-informed, and informed consent was obtained before the examination. The inclusion criteria were as follows: (a) patients who underwent US examination and US-guided fine-needle aspiration (FNA) before subtotal or total thyroidectomy; (b) nodules pathologically confirmed as PTC; and (c) patients who underwent lymph node resection. Nodules with the following criteria were excluded: (a) unclear US images, (b) insufficient puncture specimens to obtain adequate RNA, and (c) preoperative radiotherapy or chemotherapy.

2.2. Image examination

An Aplio 500 (Canon Medical Systems, Otawara, Japan) equipped with a linear array probe (14L5 probe, 5-14 MHz) was used. US imaging was performed by two radiologists with extensive experience in thyroid US diagnosis, both blinded to all histologic information and clinical history. Thyroid tumors were evaluated for internal architecture (mostly solid, solid), echogenicity (isoechoic, hypoechoic, marked hypoechoic), margin (regular, irregular), shape (wider than tall, taller than wide), calcification (none or macro, micro), peripheral halo (absent, present), capsular invasion (absent, present), and blood flow (none, low, high). In US findings, capsular invasion was defined as greater than 25% of capsule contact between thyroid nodule and capsule, obvious loss of the echogenic capsule line, or invasion of the surrounding soft tissue (*29,30*).

2.3. Specimen collection

All patients underwent US-guided FNA with a 22-gauge needle by the same radiologists who had performed the US examination previously. Aspiration was performed at least three times. Cytological tissue from the first two aspiration samples was smeared on glass slides, immediately placed in 95% alcohol, and stained for hematoxylin-eosin staining. Cytological tissue from the last aspiration was eluted with normal saline and immediately frozen in -80°C liquid nitrogen.

2.4. Cell culture and transfection

The human PTC cell lines (B-CPAP and KTC-1) were obtained from the Chinese Academy of Sciences Committee on Type Culture Collection Cell Bank (Shanghai, China). Two cell lines were cultured in RPMI-1640 medium (Gibco, Australia) supplemented with 10% of fetal bovine serum (FBS) (Gibco, Australia) and incubated at 37°C in a constant temperature incubator.

ENST00000438158 overexpression plasmid was used to upregulate ENST00000438158 expression. Small interfering RNAs (siRNAs) were obtained from GenePharma Co., Ltd. (Shanghai, China) to downregulate ENST00000438158 expression. Transfection was conducted using Lipofectamine 2000 test agent (Invitrogen, Carlsbad, CA, USA), according to the manufacturer's instructions.

2.5. Real-time quantitative PCR assays

TRIzol reagent (Invitrogen, Carlsbad, CA, USA) was used to extract total RNA from clinical tissue samples and transfected cells, according to the manufacturer's instructions. Quantitative reverse transcription polymerase chain reaction (qRT-PCR) was performed using the ChamQ Universal SYBR qPCR Master Mix (Vazyme, Nanjing, China). The relative expression levels of ENST00000438158 were calculated using the $2^{-\Delta\Delta Ct}$ method which was normalized to GAPDH.

2.6. CCK8 assay and plate clone formation assay

Cell Counting Kit-8 (CCK8; Beyotime Biotechnology, Jiangsu, China) was used to analyze the proliferation capacity of the cells. Absorbance of different time points at 450 nm was measured using a microplate reader according to which the proliferation ability curve of B-CPAP and KTC-1 cells was generated.

The effect of ENST00000438158 on PTC cell proliferation was further confirmed using a plate clone formation assay. The cells were seeded into six-well plates at a density of 500 cells/well. The medium was replaced every two days. On the tenth day, the medium was discarded. The cells were stained with crystal violet at room temperature and photographed.

2.7. Transwell assay

Transwell chambers (Corning, NY, USA) were used to determine cell migration and invasion. Matrigel was placed at the bottom of the upper chamber for invasion assay. Complete medium (500 μL) was added to the lower chamber, and 5×10^4 cells resuspended in a suitable medium with free serum were added to the upper chamber. After 24 h incubation, the cells from the upper chamber were removed. Cells that migrated or invaded the bottom surface of the membrane were stained with crystal violet, observed under a light microscope, and photographed.

2.8. Flow cytometry

The cell apoptosis assay was conducted using the Annexin V Apoptosis Detection Kit FITC (Invitrogen, NY, USA). Cell cycle analysis was performed using a Cell Cycle and Apoptosis Analysis Kit (Beyotime Biotechnology, Jiangsu, China). Cell apoptosis assay and cell cycle analysis were performed according to the manufacturer's protocol. Cell apoptosis and the cell cycle were analyzed using a Gallios Flow Cytometer (Beckman Coulter, USA) and FlowJo software.

2.9. Statistical analysis

Continuous variables are presented as mean values ± standard deviation (SD), and were compared using an independent two-sample *t*-test. Categorical variables were described as rate or frequency and compared the χ^2-test. Multivariate logistic analysis was used to analyze the significant variables in the univariate analysis. Based on pathological diagnosis, a receiver operating characteristic (ROC) curve was drawn to obtain the area under the curve (AUC), sensitivity, and specificity. The diagnostic effectiveness of the different methods was analyzed using the *z*-test.

All statistical analyses were performed using Statistical Product and Service Solutions (SPSS) 25.0 software and GraphPad Prism software (version 8.0). Differences were considered statistically significant at $p < 0.05$.

3. Results

3.1. Clinical and US Characteristics of patients

According to the pathological results, 18 and 31 patients were in the CLNM+ (PTC with CLNM) and CLNM- (PTC without CLNM) group. As shown in Table 1, sex, size, calcification, and capsule contact were significantly related to CLNM in PTC (all $p < 0.05$) (Figures 1A-1D). However, no significant differences were found in age, location, multifocality, diffuse lesions, extra-thyroid extension, internal architecture, echogenicity, margin, shape, halo, and blood between the two groups (all $p > 0.05$). Calcification (OR = 7.398) and capsule contact (OR = 6.749) were independent predictors of CLNM of PTC in the multivariate logistic regression analysis (both $p < 0.05$) (Table 2).

3.2. The expression of ENST0000438158 in FNA cytological specimen and PTC cell lines

The expression of ENST00000438158 differed significantly between the CLNM- and CLNM+ groups, with lower ENST00000438158 expression in the CLNM+ group ($p = 0.035$) (Figure 2A). In the PTC cell line, the expression of ENST00000438158 was significantly higher than that of KTC-1 in B-CPAP cells (Figure 2B). Therefore, KTC-1 was selected for the overexpression experiment, and B-CPAP was selected for the low expression test (Figures 2C-2D). To investigate the significance of ENST0000438158 expression in PTC with CLNM, receiver operator characteristic (ROC) was used to calculate the cutoff value of ENST0000438158 expression (Figure 2E). According to the best cut-off value of ΔCt = 43.71, 29 and 20 patients were in the low (ΔCt < 43.71) and high expression group (ΔCt > 43.71), respectively. ENST0000438158 expression was correlated with PTC accompanied by CLNM ($p = 0.009$) (Figures 1A-1D). However, ENST0000438158 expression was not associated with sex, age, location, size, multifocality, diffuse lesion, extrathyroidal

Table 1. Clinicopathological characteristics and ultrasound characteristics of CLNM in PTC

Variable	*n*	CLNM+, *n* (%)	CLNM-, *n* (%)	*p* value
Sex				0.001
Male	14 (28.6)	10 (55.6)	4 (12.9)	
Female	35 (71.4)	8 (44.4)	27 (87.1)	
Age				0.095
> 45	24 (49.0)	6 (33.3)	18 (58.1)	
≤ 45	25 (51.0)	12 (66.7)	13 (41.9)	
Tumor location				0.108
Left	20 (40.8)	4 (22.2)	16 (51.6)	
Right	26 (53.1)	12 (66.7)	14 (45.2)	
Isthmus	3 (6.1)	2 (11.1)	1 (3.2)	
Tumor size (mm)				0.048
≤ 10	33 (67.3)	9 (50.0)	24 (77.4)	
> 10	16 (32.4)	9 (50.0)	7 (22.6)	
Multifocality				0.925
Unifocal	35 (71.4)	13 (72.2)	22 (71.0)	
Multifocal	14 (28.6)	5 (27.8)	9 (29.0)	
Diffuse lesion				0.743
Absent	34 (69.4)	13 (72.2)	21 (67.7)	
Present	15 (30.6)	5 (27.8)	10 (32.3)	
Extra-thyroid extension				1.000
Absent	38 (77.6)	14 (77.8)	24 (77.4)	
Present	11 (22.4)	4 (22.2)	7 (22.6)	
Internal architecture				0.367
Mostly solid	1 (2.0)	1 (5.6)	0 (0)	
Solid	48 (98.0)	17 (94.4)	31 (100)	
Echogenicity				0.505
Isoechoic	1 (2.0)	0 (0)	1 (3.2)	
Hypoechoic	41 (83.7)	14 (77.8)	27 (87.1)	
Markedly hypoechoic	7 (14.3)	4 (22.2)	3 (9.7)	
Margin				0.069
Regular	16 (32.7)	3 (16.7)	13 (41.9)	
Irregular	33 (67.3)	15 (83.3)	18 (58.1)	
Shape				0.417
Wider than tall	20 (40.8)	6 (33.3)	14 (45.2)	
Taller than wide	29 (50.2)	12 (66.7)	17 (54.8)	
Calcification				0.009
None or Macro	20 (40.8)	3 (16.7)	17 (54.8)	
Micro	29 (59.2)	15 (83.3)	14 (45.2)	
Halo				1.000
Absent	36 (73.5)	13 (72.2)	23 (74.2)	
Present	13 (26.5)	5 (27.8)	8 (25.8)	
Capsular invasion				0.007
Absent	31 (63.3)	7 (38.9)	24 (77.4)	
Present	18 (36.7)	11 (61.1)	7 (22.6)	
CLNM on US				0.084
Absent	46 (93.9)	15 (83.3)	21 (100)	
Present	3 (6.1)	3 (16.7)	0 (0)	
Blood flow				0.837
None	18 (36.7)	6 (33.3)	12 (38.7)	
Low	25 (51.0)	9 (50.0)	16 (51.6)	
High	6 (12.3)	3 (16.7)	3 (9.7)	

CLNM, cervical lymph node metastasis; PTC, papillary thyroid carcinoma; CLNM+, papillary thyroid carcinoma with cervical lymph node metastasis; CLNM-, papillary thyroid carcinoma without cervical lymph node metastasis; US, ultrasound.

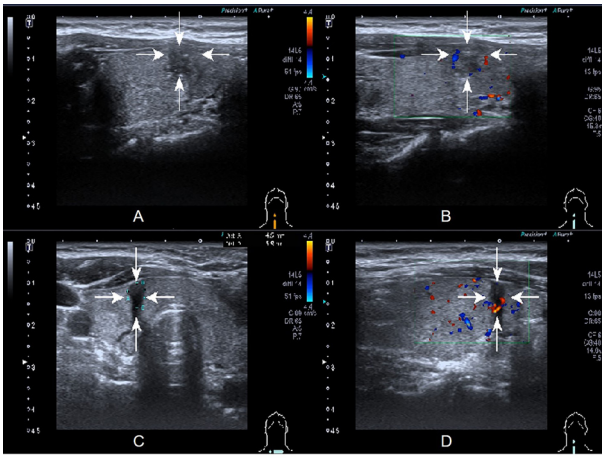

Figure 1. Examples of ultrasound features and the expression of ENST0000438158. (A) A 27-year-old female with CLNM in PTC showing low expression of ENST0000438158. US images presented with taller than wide and microcalcification; **(B)** A 30-year-old female with CLNM in PTC showing low expression of ENST0000438158. US images presented with microcalcification, 25% - 50% contact capsule and low blood supply on. **(C)** A 59-year-old female without CLNM in PTC showing high expression of ENST0000438158. US images presented with taller than wide and < 25% contact capsule. **(D)** A 53-year-old male without CLNM in PTC showing high expression of ENST0000438158. US images presented with taller than wide, < 25% contact capsule and high blood supply on.

Table 2. Multivariate logistic regression analysis to identify predictors of CLNM in PTC

Parameter	B	SE	OR	95% CI	*p* value
Size (> 10 mm)	0.768	0.741	2.155	0.504 - 9.212	0.300
Calcification(microcalcification)	2.001	0.846	7.398	1.409 - 38.845	0.018
Capsular invasion (Capsular invasion)	1.909	0.771	6.749	1.491 - 30.556	0.013
Constant	-2.913	0.872	0.054		

CLNM, cervical lymph node metastasis; PTC, papillary thyroid carcinoma; 95% CI, 95% confidence interval.

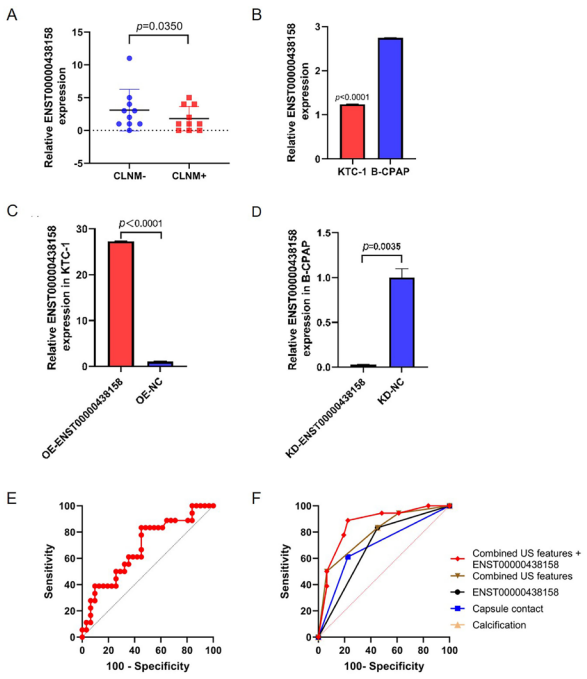

Figure 2. The expression of ENST0000438158 in PTC patients' cytological specimen and PTC cell lines. (A) The expression of ENST0000438158 in PTC tissues was detected by qRT-PCR according to CLNM in PTC. **(B)** The expression of ENST0000438158 in KTC-1 and B-CPAP cells was detected by qRT-PCR. **(C)** Overexpression of ENST00000438158 in KTC-1 cells. **(D)** Knockdown of ENST00000438158 in B-CPAP cells. **(E)** The cut-off value of ENST0000438158 expression was determined by ROC curve. **(F)** The ROC curves of US features and ENST00000438158 predicted cervical lymph node metastasis of PTC.

extension, internal architecture, echogenicity, margin, shape, calcification, halo, capsular invasion, or blood (all $p > 0.05$) (Table 3). Compared with the single US characteristics, the multiple US features were more valuable in predicting the CLNM of PTC (AUC = 0.794, 95% confidence interval (CI) = 0.654 - 0.896). The AUC of ENST0000438158 in predicting the CLNM in PTC was 0.691 (95% CI = 0.543 - 0.815). Adding ENST0000438158 to US can increase the value of predicting CLNM in PTC (AUC = 0.861, 95% CI = 0.732 - 0.943) ($p < 0.05$) (Figure 2F) (Table 4).

3.3. Effect of ENST00000438158 expression in migration and invasiveness of PTC cell lines

In transwell migration experiments, the migratory capability of KTC-1 cells was lower than that of the negative control group when ENST00000438158 expression was upregulated. In addition, the high migratory abilities of B-CPAP cells were statistically induced by downregulating ENST00000438158 compared with the negative control group (Figures 3A-3B). Transwell invasion experiments showed that overexpression of ENST00000438158 could inhibit the ability of invasion of KTC-1 cells, conversely, knockdown of ENST00000438158 could promote the invasion of B-CPAP cells (Figures 3C-3D). In summary, the expression of ENST00000438158 was closely related to the migration and invasion of PTC cells.

3.4. Role of ENST00000438158 expression on cell proliferation, apoptosis, and cell cycle in PTC

In the CCK8 assay, upregulating ENST00000438158 expression inhibited KTC-1 proliferation (Figure 4A), whereas the proliferation of B-CPAP cells was increased when the expression of ENST00000438158 was knocked down (Figure 4B). In addition, the colony formation assay showed similar results (Figures 4C-4D).

As shown in Figures 5A-5B, the percentage of apoptotic cells remarkably decreased when ENST00000438158 was knocked down. ENST00000438158 overexpression increased the proportion of apoptotic cells. Compared with the negative control group, there was no significant difference in the proportion of G1, S, and G2/M phase cells in both B-CPAP and KTC-1 cells when ENST00000438158 was knocked down or overexpressed (Figures 6A-6B).

Collectively, knockdown of ENST00000438158 expression promoted PTC cell proliferation and reduced cell apoptosis.

4. Discussion

Although PTC is an indolent cancer, it is frequently accompanied by CLNM (*5,6*). One study found that the recurrence and mortality rates of thyroid cancer with CLNM were 30 times higher than those of thyroid cancer without CLNM (*31*). Hence, CLNM is considered a high-risk factor for local recurrence and a poor prognosis, which may influence the selection of surgical procedures (*11,32*). US is the preferred method for the preoperative diagnosis of PTC and evaluation of cervical lymph nodes. In our study, only three PTC

Table 3. Correlations between ENST0000438158 expression, clinicopathological characteristics and ultrasound characteristics of PTC

Variable	*n*	Low expression, *n* (%)	High expression, *n* (%)	*p* value
Sex				0.646
Male	14 (28.6)	9 (31.0)	5 (25.0)	
Female	35 (71.4)	20 (69.0)	15 (75.0)	
Age				0.200
> 45	24 (49.0)	12 (41.4)	12 (60.0)	
≤ 45	25 (51.0)	17 (58.6)	8 (40.0)	
Tumor location				0.897
Left	20 (40.8)	11 (37.9)	9 (45.0)	
Right	26 (53.1)	16 (55.2)	10 (50.0)	
Isthmus	3 (6.1)	2 (6.9)	1 (5.0)	
Tumor size (mm)				0.343
≤ 10	33 (67.3)	18 (62.1)	15 (75.0)	
> 10	16 (32.4)	11 (37.9)	5 (25.0)	
Multifocality				0.141
Unifocal	35 (71.4)	23 (79.3)	12 (60.0)	
Multifocal	14 (28.6)	6 (20.7)	8 (40.0)	
Diffuse lesion				0.479
Absent	34 (69.4)	19 (65.5)	15 (75.0)	
Present	15 (30.6)	10 (34.5)	5 (25.0)	
Extra-thyroid extension				0.740
Absent	38 (77.6)	23 (79.3)	15 (75.0)	
Present	11 (22.4)	6 (20.7)	5 (25.0)	
Internal architecture				1.000
Mostly solid	1 (2.0)	1 (3.4)	0 (0.0)	
Solid	48 (98.0)	28 (96.6)	20 (100.0)	
Echogenicity				0.662
Isoechoic	1 (2.0)	1 (3.4)	0 (0.0)	
Hypoechoic	41 (83.7)	25 (86.2)	16 (80.0)	
Markedly hypoechoic	7 (14.3)	3 (10.4)	4 (20.0)	
Margin				0.771
Regular	16 (32.7)	9 (31.0)	7 (35.0)	
Irregular	33 (67.3)	20 (69.0)	13 (65.0)	
Shape				0.491
Wider than tall	20 (40.8)	13 (44.8)	7 (35.0)	
Taller than wide	29 (50.2)	16 (55.2)	13 (65.0)	
Calcification				0.621
None or Macro	20 (40.8)	11 (37.9)	9 (45.0)	
Micro	29 (59.2)	18 (62.1)	11 (55.0)	
Halo				0.840
Absent	36 (73.5)	21 (72.4)	15 (75.0)	
Present	13 (26.5)	8 (27.6)	5 (25.0)	
Capsular invasion				0.417
Absent	31 (63.3)	17 (58.6)	14 (70.0)	
Present	18 (36.7)	12 (41.4)	6 (30.0)	
Blood flow				0.124
None	18 (36.7)	7 (24.1)	11 (55.0)	
Low	25 (51.0)	18 (62.1)	7 (35.0)	
High	6 (12.3)	4 (13.8)	2 (10.0)	
CLNM				0.009
CLNM-	31 (63.3)	14 (48.3)	17 (85.0)	
CLNM+	18 (36.7)	15 (51.7)	3 (15.0)	

CLNM, cervical lymph node metastasis; PTC, papillary thyroid carcinoma; CLNM+, papillary thyroid carcinoma with cervical lymph node metastasis; CLNM-, papillary thyroid carcinoma without cervical lymph node metastasis.

Table 4. Combined diagnostic value of ENST00000438158 with ultrasound of CLNM in PTC

Variable	Critical value	AUC (95% CI)	Sensitivity (%)	Specificity (%)
ENST00000438158	Low expression	0.691 (0.543 - 0.815)	83.3	54.8
Capsule contact	≥25%	0.693 (0.545 - 0.816)	61.11	77.42
Calcification	Microcalcification	0.691 (0.543 - 0.815)	83.33	54.84
Combined US features	Combined US features	0.794 (0.654 - 0.896)	50.00	93.55
Combined US features + ENST00000438158	Combined US features + ENST00000438158	0.861 (0.732 - 0.943)	88.89	77.42

CLNM, cervical lymph node metastasis; PTC, papillary thyroid carcinoma. 95% CI, 95% confidence interval.

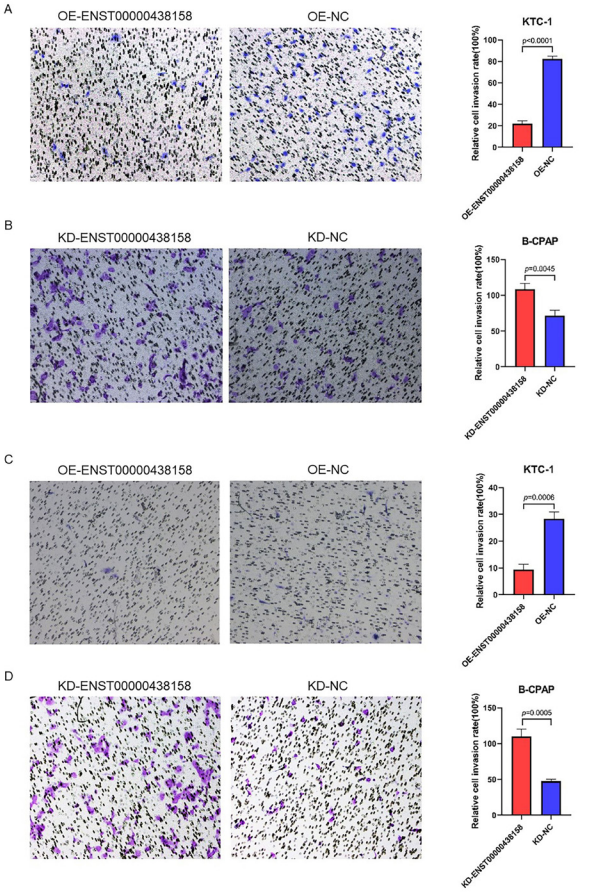

Figure 3. Effect of ENST00000438158 on the migration and invasiveness of PTC celllines. A Transwell assay was performed to determine the migration ability of **(A)** KTC-1 cells and **(B)** B-CPAP cells. A Transwell assay was performed to determine the invasion ability of **(C)** KTC-1 cells and **(D)** B-CPAP cells. Representative images show migrated cells and invasive cells stained with crystal violet. The quantification of cell migration and invasion is presented as number of migrating and invading cells. All experiments were performed independently in triplicate.

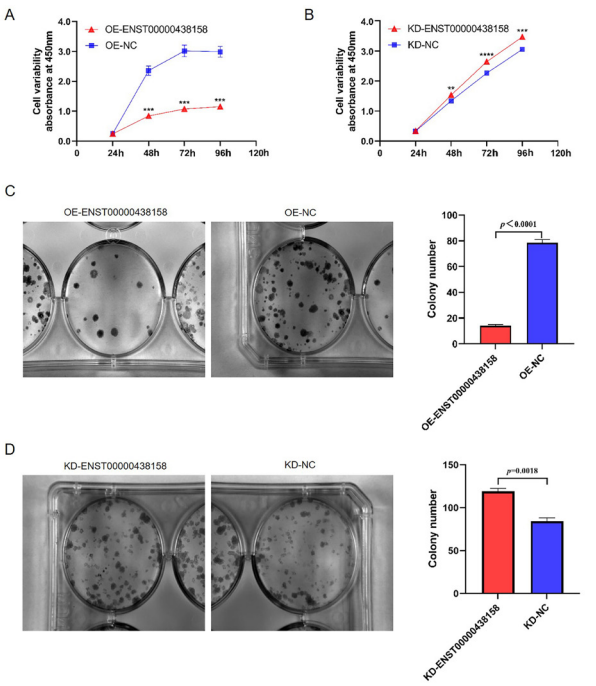

Figure 4. Effect of ENST00000438158 on the proliferation of PTC cell lines. A CCK-8 assay was performed to determine the proliferation of **(A)** KTC-1 cells and **(B)** B-APAP cells. A colony formation assay was performed to determine the proliferation of **(C)** KTC-1 cells and **(D)** B-APAP cells. The colonies were captured and counted and the results were presented in the histogram. All experiments were performed independently in triplicate.

patients with CLNM were detected by US, with 16.7% sensitivity. A similar result has been reported in other studies (*12-14*). Considering the higher prevalence of CLNM and the poor performance of US in preoperative detection of CLNM, it is necessary to predict CLNM with US features of primary PTC. Some scholars have found that greater than 25% of capsule contact with thyroid nodules is a useful index to predict the CLNM of PTC, with 74.3-86.2% sensitivity and 55.3-66.1% specificity (*33,34*), which is consistent with the findings of our study. This is because the thyroid gland is surrounded by a capsule with abundant lymphatic vessels. The closer the lesion is to the capsule, the greater the risk of contact between the cancer tissue and lymphatic vessels, and the probability of lymphatic metastasis to lymph nodes increases. The mechanism of microcalcification in thyroid cancer may be caused by excessive hyperplasia of fibrous tissue and blood vessels in the nodules. However, Das *et al.* (*35*) proposed that the sand precursor in the pericarp was released into local tissues by intact tumor cells and then calcified; therefore, the sand precursor (microcalcification on imaging) represented an active biological process rather than dystrophic calcification or tumor cell death. The current study also indicated that microcalcification was associated with CLNM, which is in accordance with results of previous studies (*36,37*). Furthermore, we performed an analysis of single US features and multiple US features combined to predict PTC with CLNM. The results showed that the value of combining multiple US features to predict PTC with CLNM was higher than that of a single US feature, but its sensitivity was still low. Xia *et al.* (*38*) also analyzed the value of US features in diagnosing CLNM of PTC and presented high specificity but low sensitivity, which was consistent with our results.

FNA is an effective method to predict CLNM in PTC, with 73-94% sensitivity. The main reason for this is that FNA largely depends on the experience and ability of the operators and cell pathologists (*39,40*). In addition, the small size of lymph nodes and the interference of lymphocyte infiltration and internal necrosis also affect FNA results (*40,41*). To overcome the limitations of imaging and cytology, the detection of molecular markers has become the focus of current research. Diaz *et al.* (*42*) compared the diagnostic value of FNA alone and FNA combined with detection of

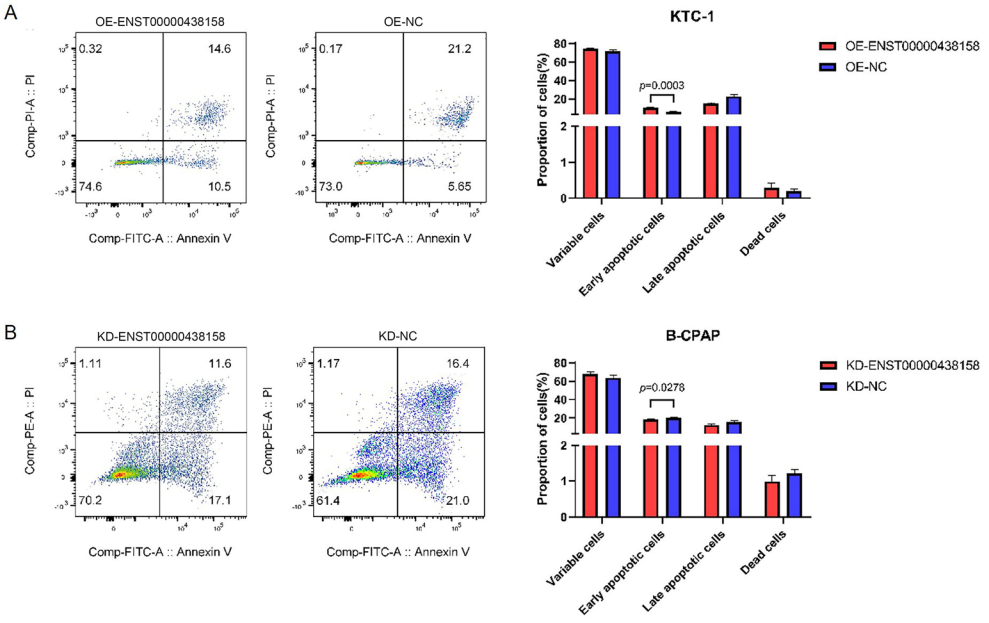

Figure 5. Effect of ENST00000438158 on the apoptosis of PTC cell lines. Flow cytometric analysis of apoptosis in **(A)** KTC-1 cells and **(B)** B-APAP cells. The percentage of apoptotic cells was presented in the histogram. Data were expressed as the means ± SD of three independent experiments.

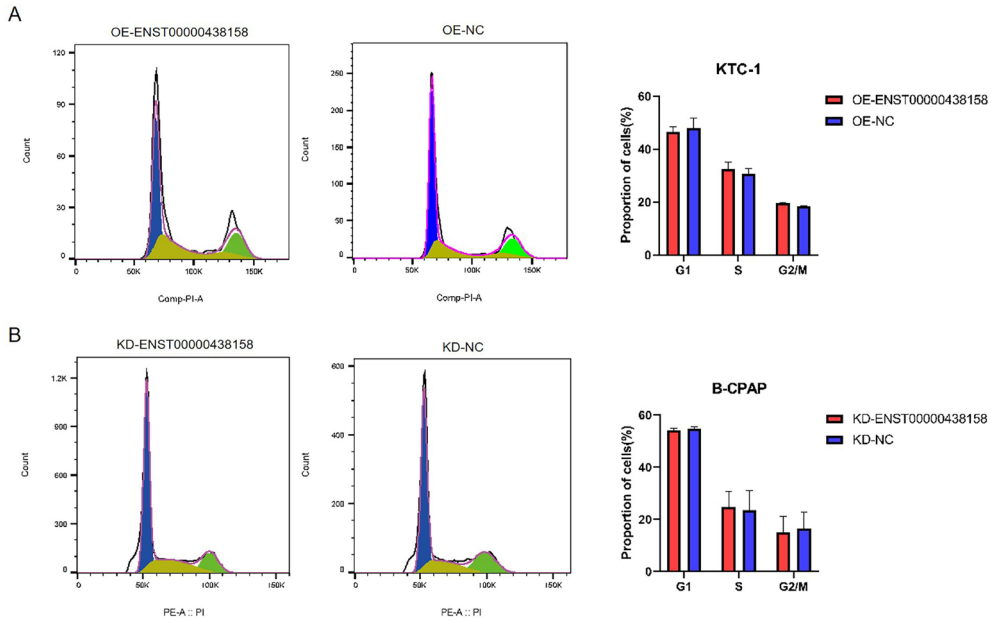

Figure 6. Effect of ENST00000438158 on the cell cycle status of PTC cell lines. Flow cytometric analysis of the cell cycle in **(A)** KTC-1 cells and **(B)** B-APAP cells. Results quantified in the cell cycle analysis were shown as a percentage of the total number of cells. Data were expressed as the means ± SD of three independent experiments.

KI-67 in pancreatic endocrine tumors, and the results showed that the latter method had a higher diagnostic value. Li *et al.* (*43*) evaluated the value of lymph node FNA alone and combined with thyroglobulin detection in PTC with CLNM, and the results also showed that the combined detection had higher accuracy. Therefore, FNA combined with the detection of molecular markers can not only obtain cytology samples but also carry out molecular diagnostic information at the same time, which has a certain guiding significance for clinical use. In our study, PTC primary lesions were punctured rather than cervical lymph nodes, with the advantage of avoiding injury to the cervical blood vessels and nerve sheath to reduce operational risk.

At present, some researchers have found that lncRNAs have certain clinical guiding potential

in various tumors, and it may become an effective biomarker (*44,45*). Some studies, such as HOTAIR (*46*) and ANRIL (*47*), have shown that lncRNAs can effectively predict CLNM in PTC. Xia *et al.* (*38*) indicated that the expression level of NONHSAT076754 was positively correlated with CLNM in PTC and clinical stage. Zheng *et al.* (*48*) showed that an increase in BANCR expression is associated with poor prognosis, CLNM, and distant metastasis by regulating the expression of TSHR and its downstream cyclin D1. Previous studies have confirmed that ENST0000438158 is associated with the occurrence, development, and lung metastasis of osteosarcoma (*28*). It has been reported that lncRNAs may act as endogenous "sponges," which downregulate a series of miRNA activities, affecting the occurrence and development of thyroid cancer (*49,50*). We assume that ENST00000438158 may function as a "sponge," competitively binding to miRNAs, and regulating the occurrence and development of PTC. In our study, we confirmed that ENST0000438158 is negatively associated with CLNM in PTC. Furthermore, an *in vitro* functional study demonstrated that knockdown or upregulation of ENST0000438158 expression promotes or inhibits the proliferation, migration, and invasion of PTC cells. Because of the low sensitivity of US in predicting CLNM, we adopted a combination of US features and the expression of ENST0000438158 to improve diagnostic sensitivity. When ENST0000438158 was added to the US, the value of differentiating PTC from CLNM was greatly improved, and the AUC, sensitivity, and specificity of combined ENST00000438158 and US were 0.861, 88.89%, and 77.42%, respectively. Therefore, preoperative detection of ENST0000438158 expression is of great importance. The rate of missed diagnoses can be reduced by combining the US and ENST0000438158.

However, this study has some limitations. First, a small number of PTC cases were recruited in this study, which can be further studied by expanding the number of specimens over the long term. Second, the mechanism by which ENST0000438158 regulates CLNM in PTC was not elucidated in our study. Therefore, further studies on this mechanism are needed to provide guidance for clinical practice.

In conclusion, the low expression of ENST0000438158 was related to CLNM in PTC, which can promote cell proliferation, metastasis, and invasion, while inhibiting apoptosis. Adding ENST0000438158 to US can increase the diagnostic value of predicting PTC with CLNM. Therefore, ENST0000438158 may be a promising auxiliary diagnostic biomarker to be combined with US for the prediction of CLNM in PTC.

Acknowledgements

The authors wish to sincerely thank Peng Li and Suna Tian for their assistance in preparing the figures in this manuscript.

Funding: This work was supported by the Shanghai Municipal Health and Family Planning Commission of China (grant number 201640285 to L Chen), a project under the Scientific and Technological Innovation Action Plan of the Shanghai Natural Science Fund (grant no. 20ZR1409100 to L Wang), and a project of the Chinese Association of Integration of Traditional and Western Medicine Special Foundation for Obstetrics and Gynecology-PuZheng Pharmaceutical Foundation (grant no. FCK-PZ-08 to L Wang), a project for hospital management of the Shanghai Hospital Association (grant no. X2021046 to L Wang), and a clinical trial project of the Special Foundation for Healthcare Research of the Shanghai Municipal Health Commission (Grant No. 202150042 to L Wang).

Conflict of Interest: The authors have no conflicts of interest to disclose.

References

1. Siegel RL, Miller KD, Jemal A. Cancer statistics, 2020. CA Cancer J Clin. 2020; 70:7-30.
2. Rahib L, Smith BD, Aizenberg R, Rosenzweig AB, Fleshman JM, Matrisian LM. Projecting cancer incidence and deaths to 2030: The unexpected burden of thyroid, liver, and pancreas cancers in the United States. Cancer Res. 2014; 74:2913-2921.
3. Lim H, Devesa SS, Sosa JA, Check D, Kitahara CM. Trends in thyroid cancer incidence and mortality in the United States, 1974-2013. JAMA. 2017; 317:1338-1348.
4. Kitahara CM, Sosa JA. The changing incidence of thyroid cancer. Nat Rev Endocrinol. 2016; 12:646-653.
5. Al-Brahim N, Asa SL. Papillary thyroid carcinoma: An overview. Arch Pathol Lab Med. 2006; 130:1057-1062.
6. Ito Y, Kihara M, Takamura Y, Kobayashi K, Miya A, Hirokawa M, Miyauchi A. Prognosis and prognostic factors of papillary thyroid carcinoma in patients under 20 years. Endocr J. 2012; 59:539-545.
7. Viola D, Agate L, Molinaro E, Bottici V, Lorusso L, Latrofa F, Torregrossa L, Boldrini L, Ramone T, Vitti P, Elisei R. Lung recurrence of papillary thyroid cancer diagnosed with antithyroglobulin antibodies after 10 years from initial treatment. Front Endocrinol (Lausanne). 2018; 9:590.
8. Mazzaferri EL, Jhiang SM. Long-term impact of initial surgical and medical therapy on papillary and follicular thyroid cancer. Am J Med. 1994; 97:418-428.
9. So YK, Kim MJ, Kim S, Son YI. Lateral lymph node metastasis in papillary thyroid carcinoma: A systematic review and meta-analysis for prevalence, risk factors, and location. Int J Surg. 2018; 50:94-103.
10. Sturgeon C, Yang A, Elaraj D. Surgical management of lymph node compartments in papillary thyroid cancer. Surg Oncol Clin N Am. 2016; 25:17-40.
11. Haugen BR, Alexander EK, Bible KC, *et al.* 2015 American thyroid association management guidelines for adult patients with thyroid nodules and differentiated thyroid cancer: The American thyroid association guidelines task force on thyroid nodules and differentiated

thyroid cancer. Thyroid. 2016; 26:1-133.
12. Zhao H, Li H. Meta-analysis of ultrasound for cervical lymph nodes in papillary thyroid cancer: Diagnosis of central and lateral compartment nodal metastases. Eur J Radiol. 2019; 112:14-21.
13. Baek SK, Jung KY, Kang SM, Kwon SY, Woo JS, Cho SH, Chung EJ. Clinical risk factors associated with cervical lymph node recurrence in papillary thyroid carcinoma. Thyroid. 2010; 20:147-152.
14. Moo TA, McGill J, Allendorf J, Lee J, Fahey T, Zarnegar R. Impact of prophylactic central neck lymph node dissection on early recurrence in papillary thyroid carcinoma. World J Surg. 2010; 34:1187-1191.
15. Xu Y, Yang X, Si T, Yu H, Li Y, Xing W, Guo Z. MCM4 in human hepatocellular carcinoma: A potent prognostic factor associated with cell proliferation. Biosci Trends. 2021; 15:100-106.
16. Zhu J, Zhao R, Xu W, Ma J, Ning X, Ma R, Meng F. Correlation between reticulum ribosome-binding protein 1 (RRBP1) overexpression and prognosis in cervical squamous cell carcinoma. Biosci Trends. 2020; 14:279-284.
17. Flynn RA, Chang HY. Long noncoding RNAs in cell-fate programming and reprogramming. Cell Stem Cell. 2014; 14:752-761.
18. Mercer TR, Dinger ME, Mattick JS. Long non-coding RNAs: Insights into functions. Nat Rev Genet. 2009; 10:155-159.
19. Lin X, Qiu J, Hua K. Long non-coding RNAs as emerging regulators of epithelial to mesenchymal transition in gynecologic cancers. Biosci Trends. 2018; 12:342-353.
20. Gu Y, Xiao X, Yang S. LncRNA MALAT1 acts as an oncogene in multiple myeloma through sponging miR-509-5p to modulate FOXP1 expression. Oncotarget. 2017; 8:101984-101993.
21. Zuo Y, Li Y, Zhou Z, Ma M, Fu K. Long non-coding RNA MALAT1 promotes proliferation and invasion *via* targeting miR-129-5p in triple-negative breast cancer. Biomed Pharmacother. 2017; 95:922-928.
22. Hu Y, Deng C, Zhang H, Zhang J, Peng B, Hu C. Long non-coding RNA XIST promotes cell growth and metastasis through regulating miR-139-5p mediated Wnt/β-catenin signaling pathway in bladder cancer. Oncotarget. 2017; 8:94554-94568.
23. Ding J, Wang F, Xiang T, Qiao M. Expression and function of long noncoding RNA NONHSAT129183 in papillary thyroid cancer. Oncol Res. 2018; 26:1047-1053.
24. Zuo Z, Liu L, Song B, Tan J, Ding D, Lu Y. Silencing of long non-coding RNA ENST00000606790.1 inhibits the malignant behaviors of papillary thyroid carcinoma through the PI3K/AKT pathway. Endocr Res. 2021; 46:1-9.
25. Guo LJ, Zhang S, Gao B, Jiang Y, Zhang XH, Tian WG, Hao S, Zhao JJ, Zhang G, Hu CY, Yan J, Luo DL. Low expression of long non-coding RNA GAS5 is associated with poor prognosis of patients with thyroid cancer. Exp Mol Pathol. 2017; 102:500-504.
26. Wang C, Yan G, Zhang Y, Jia X, Bu P. Long noncoding RNA MEG3 suppresses migration and invasion of thyroid carcinoma by targeting of Rac1. Neoplasma. 2015; 62:541-549.
27. Luo J, Xu L, Jiang Y, Zhuo D, Zhang S, Wu L, Xu H, Huang Y. Expression profile of long non-coding RNAs in colorectal cancer: A microarray analysis. Oncol Rep. 2016; 35:2035-2044.
28. Xie L, Yao Z, Zhang Y, Li D, Hu F, Liao Y, Zhou L, Zhou Y, Huang Z, He Z, Han L, Yang Y, Yang Z. Deep RNA sequencing reveals the dynamic regulation of miRNA, lncRNAs, and mRNAs in osteosarcoma tumorigenesis and pulmonary metastasis. Cell Death Dis. 2018; 9:772.
29. Kim H, Kim JA, Son EJ, Youk JH, Chung TS, Park CS, Chang HS. Preoperative prediction of the extrathyroidal extension of papillary thyroid carcinoma with ultrasonography versus MRI: A retrospective cohort study. Int J Surg. 2014; 12:544-548.
30. Kim H, Kim JA, Son EJ, Youk JH. Quantitative assessment of shear-wave ultrasound elastography in thyroid nodules: Diagnostic performance for predicting malignancy. Eur Radiol. 2013; 23:2532-2537.
31. Noguchi M, Kumaki T, Taniya T, Miyazaki I. Bilateral cervical lymph node metastases in well-differentiated thyroid cancer. Arch Surg. 1990; 125:804-806.
32. Pisanu A, Reccia I, Nardello O, Uccheddu A. Risk factors for nodal metastasis and recurrence among patients with papillary thyroid microcarcinoma: Differences in clinical relevance between nonincidental and incidental tumors. World J Surg. 2009; 33:460-468.
33. Moon HJ, Sung JM, Kim EK, Yoon JH, Youk JH, Kwak JY. Diagnostic performance of gray-scale US and elastography in solid thyroid nodules. Radiology. 2012; 262:1002-1013.
34. Choi JS, Kim J, Kwak JY, Kim MJ, Chang HS, Kim EK. Preoperative staging of papillary thyroid carcinoma: Comparison of ultrasound imaging and CT. AJR Am J Roentgenol. 2009; 193:871-878.
35. Das DK. Psammoma body: A product of dystrophic calcification or of a biologically active process that aims at limiting the growth and spread of tumor? Diagn Cytopathol. 2009; 37:534-541.
36. Li F, Pan D, He Y, Wu Y, Peng J, Li J, Wang Y, Yang H, Chen J. Using ultrasound features and radiomics analysis to predict lymph node metastasis in patients with thyroid cancer. BMC Surg. 2020; 20:315.
37. Liu J, Zheng D, Li Q, Tang X, Luo Z, Yuan Z, Gao L, Zhao J. A predictive model of thyroid malignancy using clinical, biochemical and sonographic parameters for patients in a multi-center setting. BMC Endocr Disord. 2018; 18:17.
38. Xia S, Wang C, Ni X, Ni Z, Dong Y, Zhan W. NONHSAT076754 aids ultrasonography in predicting lymph node metastasis and promotes migration and invasion of papillary thyroid cancer cells. Oncotarget. 2017; 8:2293-2306.
39. Frasoldati A, Toschi E, Zini M, Flora M, Caroggio A, Dotti C, Valcavi R. Role of thyroglobulin measurement in fine-needle aspiration biopsies of cervical lymph nodes in patients with differentiated thyroid cancer. Thyroid. 1999; 9:105-111.
40. Frasoldati A, Valcavi R. Challenges in neck ultrasonography: Lymphadenopathy and parathyroid glands. Endocr Pract. 2004; 10:261-268.
41. Hall TL, Layfield LJ, Philippe A, Rosenthal DL. Sources of diagnostic error in fine needle aspiration of the thyroid. Cancer. 1989; 63:718-725.
42. Diaz Del Arco C, Diaz Perez JA, Ortega Medina L, Sastre Valera J, Fernandez Acenero MJ. Reliability of Ki-67 determination in FNA samples for grading pancreatic neuroendocrine tumors. Endocr Pathol. 2016; 27:276-283.
43. Li J, Zhang K, Liu X, Hao F, Liu Z, Wang Z. Cervical lymph node thyroglobulin measurement in washout of

fine-needle aspirates for diagnosis of papillary thyroid cancer metastases. Br J Biomed Sci. 2016; 73:79-83.
44. Nagasawa M, Tomimatsu K, Terada K, Kondo K, Miyazaki K, Miyazaki M, Motooka D, Okuzaki D, Yoshida T, Kageyama S, Kawamoto H, Kawauchi A, Agata Y. Long non-coding RNA MANCR is a target of BET bromodomain protein BRD4 and plays a critical role in cellular migration and invasion abilities of prostate cancer. Biochem Biophys Res Commun. 2020; 526:128-134.
45. Shen S, Li K, Liu Y, Liu X, Liu B, Ba Y, Xing W. Silencing lncRNA AGAP2-AS1 upregulates miR-195-5p to repress migration and invasion of EC cells *via* the decrease of FOSL1 expression. Mol Ther Nucleic Acids. 2020; 20:331-344.
46. Di W, Li Q, Shen W, Guo H, Zhao S. The long non-coding RNA HOTAIR promotes thyroid cancer cell growth, invasion and migration through the miR-1-CCND2 axis. Am J Cancer Res. 2017; 7:1298-1309.
47. Zhao JJ, Hao S, Wang LL, Hu CY, Zhang S, Guo LJ, Zhang G, Gao B, Jiang Y, Tian WG, Luo DL. Long non-coding RNA ANRIL promotes the invasion and metastasis of thyroid cancer cells through TGF-β/Smad signaling pathway. Oncotarget. 2016; 7:57903-57918.
48. Zheng H, Xu J, Hao S, Liu X, Ning J, Song X, Jiang L, Liu Z. Expression of BANCR promotes papillary thyroid cancer by targeting thyroid stimulating hormone receptor. Oncol Lett. 2018; 16:2009-2015.
49. Liang L, Xu J, Wang M, Xu G, Zhang N, Wang G, Zhao Y. LncRNA HCP5 promotes follicular thyroid carcinoma progression via miRNAs sponge. Cell Death Dis. 2018; 9:372.
50. Lin Y, Jiang J. Long non-coding RNA LINC00704 promotes cell proliferation, migration, and invasion in papillary thyroid carcinoma via miR-204-5p/HMGB1 axis. Open Life Sci. 2020; 15:561-571.

Received August 8, 2022; Revised October 10, 2022; Accepted October 12, 2022.

[§]These authors contributed equally to this work.

**Address correspondence to:*
Ling Wang, Laboratory for Reproductive Immunology, Obstetrics and Gynecology Hospital of Fudan University, 419 Fangxie Road, Shanghai, China 200011.
E-mail: Dr.wangling@fudan.edu.cn

Lin Chen, Department of Ultrasound, Huadong Hospital of Fudan University, 211 West Yan'an Rd, Shanghai, China 200040.
E-mail: linchen11@fudan.edu.cn

Released online in J-STAGE as advance publication October 19, 2022.